Characterization of bed levels with statistical equivalency

J. Sieben

Project manager river engineering, Rijkswaterstaat RIZA, Gildemeesterplein 1 , P.O. Box 9072
a.sieben@riza.rws.minvenw.nl

Abstract
To enable efficient analyses of relatively slower dynamics in bed-form averaged levels and rapid changes in bed form parameters, a procedure is developed to generate morphological parameters that are statistically equivalent to observed bed levels in domains of the river bed. This procedure provides an efficient tool to automatically construct model-oriented databases from echo sounded bed levels. Further research should expand the physical interpretation of the resulting parameters and explore the applicability in hydraulic and morphological modelling.

1. Introduction
The river Waal in the Netherlands, with a summer bed of approximately 80 km length and 260 m width, is considered an important waterway between the Rotterdam harbour and the hinterland. Maintenance of this navigation route focuses on rapid changes due to passing bed forms as well as slower changes in bed-form averaged crossings and bend-profiles. Therefore, along the river Waal, dredging operations or river engineering structures should account for morphodynamics on both scales (e.g. Sloff *et al.* (2002)). However, due to a lack of detailed prototype knowledge, prediction tools for such bed level changes are limited (e.g. De Vries *et al.* 1995). During this decade, databases of accurate bed level observations from vessel-mounted multi-beam echo soundings have become available. To process these relatively large databases, an efficient concept is suggested that generates the proper information on morphodynamics at the small time scale of bed forms and the larger time scale of bed-form averaged levels.

2. Approach
Conform most modelling concepts for river morphology, bed levels are described as the sum of a linearly varying $\hat{z}(x,y,t)$ and a fluctuation $z'(x,y,t)$. This is illustrated in the outer bend profile of Fig.1. In general, process-based models (e.g. Sloff *et al.*, 2003) are used to simulate changes in $\hat{z}(x,y,t)$, whereas a representative fluctuation $z'(x,y,t)$ is estimated by statistical analyses (e.g. Nordin, 1971) or empirical predictors (e.g. Van Rijn, 1984).

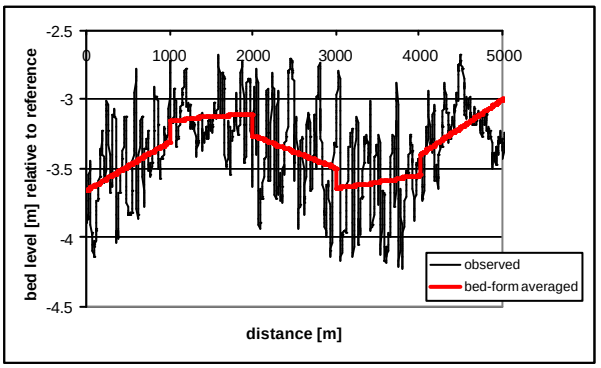

Figure 1 Illustration of a linearly varying and a fluctuating component.

The distinction of fluctuations from bed-form averaged bed levels is based on discretizing the river bed in flow-oriented domains. Within such a rectangular domain with index i, length L_x and width L_y the observed bed level $z(x,y)$ is defined as

$$z(x,y) = z'_i(x,y) + \hat{z}_i + (x - x_i)\frac{\Delta \hat{z}_i}{\Delta x} + (y - y_i)\frac{\Delta \hat{z}_i}{\Delta y} \qquad \textbf{(1)}$$

With $\hat{z}_i = \frac{1}{L_x L_y} \iint_{\Delta y \Delta x} z(x,y)\,dx dy$ domain-averaged bed level

$\frac{\Delta \hat{z}_i}{\Delta x}; \frac{\Delta \hat{z}_i}{\Delta y}$ spatial gradient of $\hat{z}_i$ in x and y direction

$z'_i(x,y)$ deviation between observed and linearly varying level

For representing z'_i, the fluctuations in one domain, a periodic model-signal is arbitrarily defined as

$$z'_i(x,y) = \frac{H}{2} \sin\left(2p \frac{s}{L}\right) \quad ; \quad s = y \sin a + x \cos a \qquad \textbf{(2)}$$

Here, H, L and $\langle$ are representative amplitude, wave length and orientation respectively (Fig.2-a). The model signal should statistically be equivalent to the fluctuations in observed bed levels. To satisfy a zero contribution of fluctuations to averaged bed levels, one would expect the length of averaging to be a multiple of L. This, however, is not necessary since modelling with Eq.2 is aiming at statistical equivalency only, implying that H, L and $\langle$ can be assumed independent of domain dimensions. Note that in stead of a sine function, a periodic triangular-shaped signal can be used as well, if this enables a physically better interpretation.

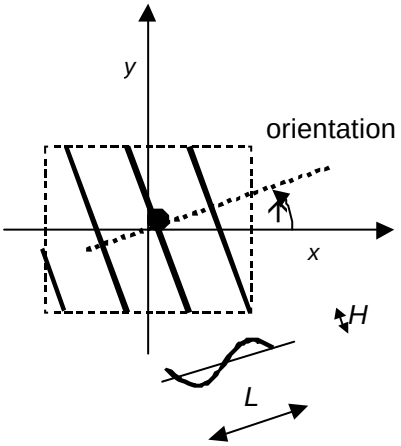

Figure 2-a Definition of model signal.

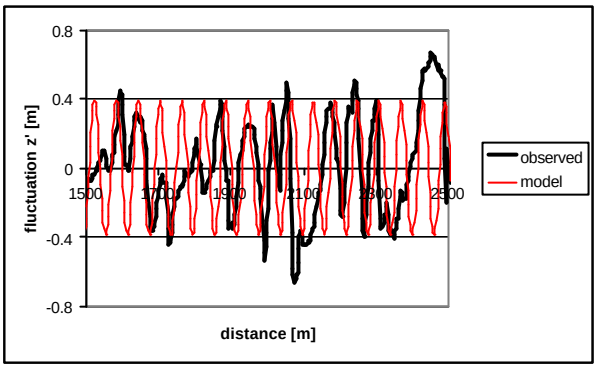

Figure 2-b Illustration of model signal and observed fluctuations.

The first parameter of the model signal is the representative amplitude H, which is determined as follows. With Eq.1, the standard deviation of observed levels in a domain can be written as

$$s_z^2 = \frac{1}{L_x L_y} \iint_{\Delta y \Delta x} (z(x,y) - \hat{z}_i)^2 dx dy \qquad \textbf{(3)}$$

After substitution of the model (Eqs 1 and 2) Eq.3 is approximated by

$$\frac{H^2}{8} \approx s_z^2 - \hat{s}_z^2 \quad ; \quad \hat{s}_z^2 = \frac{1}{12}\left(\left(L_x \frac{\Delta \hat{z}_i}{\Delta x}\right)^2 + \left(L_y \frac{\Delta \hat{z}_i}{\Delta y}\right)^2\right) \qquad \textbf{(4)}$$

This approximation is valid if the amplitude H is large relative to the spatial change in $\hat{z}_i$ over a wave length L, or $H >> \frac{4}{p} L \left| \cos a \frac{\Delta \hat{z}_i}{\Delta x} + \sin a \frac{\Delta \hat{z}_i}{\Delta y} \right|$ **(5)**

Eq.4 enables computing H from the standard deviation s_z, if $\hat{s}_z$ the contribution of gradients in $\hat{z}_i$, is determined with $\hat{z}_j$ values from neighbouring domains.

The second parameter of the model signal (Eq.2) is the wave length L. To determine this length, gradients in observed bed level (Eq.1) can be written as

$$\frac{\partial z(x,y)}{\partial x} = \frac{\partial z'_i(x,y)}{\partial x} + \frac{\Delta \hat{z}_i}{\Delta x} \text{ and } \frac{\partial z(x,y)}{\partial y} = \frac{\partial z'_i(x,y)}{\partial y} + \frac{\Delta \hat{z}_i}{\Delta y} \qquad \textbf{(6)}$$

With the model signal Eq.2 substituted in the right-hand side of Eq.6, the standard deviations of these gradients in observed bed level can be rewritten as

$$s_{zx}^2 = \frac{1}{2}\left(\cos\alpha \frac{pH}{L}\right)^2 \text{ and } s_{zy}^2 = \frac{1}{2}\left(\sin\alpha \frac{pH}{L}\right)^2 \quad \textbf{(7)}$$

Now, the wave length can be solved with $L = \frac{p}{\sqrt{2}} \frac{H}{\sqrt{s_{zx}^2 + s_{zy}^2}}$ **(8)**

It is noted that the spacing between observed bed levels should be smaller than 0.15 *L* to reduce discretization errors. It can be shown (e.g. Cramér and Leadbetter (1967); Nordin (1971)) that the wave length *L* according to Eq.8 is related to the second-derivative of the normalized auto-covariance function r as $L = 2p\left(-\frac{\mathrm{d}^2 r(0)}{\mathrm{d}t^2}\right)^{-1/2}$ **(9)**

This is illustrated in Fig.3.

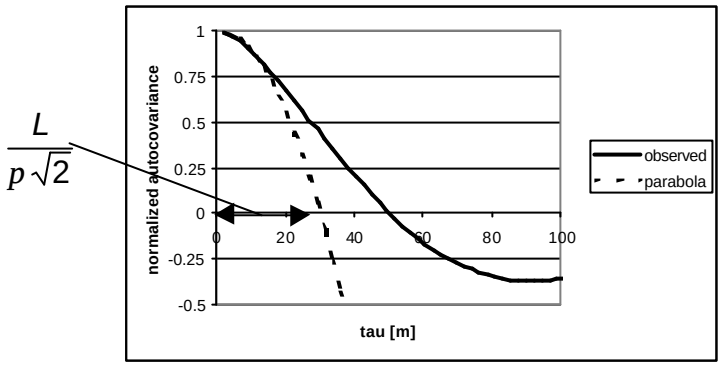

Figure 3 Relation between wave length L and normalized auto-covariance function.

The third parameter of the model signal concerns the orientation ⟨ (Fig.2-a). With Eq.6 it can be defined $Z = \frac{\partial z(x,y)}{\partial x} - \frac{\partial z(x,y)}{\partial y} = \frac{\partial z'_i(x,y)}{\partial x} - \frac{\partial z'_i(x,y)}{\partial y} + \frac{\Delta \hat{z}_i}{\Delta x} - \frac{\Delta \hat{z}_i}{\Delta y}$ **(10)**

Again, with the model signal Eq.2 substituted in the right-hand side of Eq.10, the standard deviation of Z is $s_Z^2 = \frac{1}{2}(\cos\alpha - \sin\alpha)^2\left(\frac{pH}{L}\right)^2$ **(11)**

With Eq. 8 this can be written as $\sin 2\alpha = 1 - \frac{s_Z^2}{s_{zx}^2 + s_{zy}^2}$ **(12)**

Now a representative amplitude, wave length and orientation can be found for each domain of a single set of observed bed levels. Additionally, the concept can be applied to changes in bed level observed during a period. Therefore, a migration rate *c* is defined by differentiating the model signal Eq.2 yielding

$$\frac{\partial z'_i(x,y)}{\partial t} = p\,\frac{cH}{L}\cos\left(2p\,\frac{s}{L}\right) \quad ; \quad c = \frac{\mathrm{d}s}{\mathrm{d}t} \quad \textbf{(13)}$$

Differentiation of Eq.1 yields

$$\frac{\partial z(x,y)}{\partial t} = \frac{\partial z'_i(x,y)}{\partial t} + \frac{\partial \hat{z}_i}{\partial t} + (x - x_i)\frac{\partial \Delta\hat{z}_i / \Delta x}{\partial t} + (y - y_i)\frac{\partial \Delta\hat{z}_i / \Delta y}{\partial t} \quad \textbf{(14)}$$

Analogous to Eqs 4 and 5 a standard deviation s_{zt} of changes in bed level can be determined with Eq.14. After substitution of Eq.13, it can be found

$$\frac{1}{2}\left(p\,\frac{cH}{L}\right)^2 \approx s_{zt}^2 - \hat{s}_{zt}^2 \quad ; \quad \hat{s}_{zt}^2 = \frac{1}{12}\left(\left(L_x \frac{\partial \Delta\hat{z}_i / \Delta x}{\partial t}\right)^2 + \left(L_y \frac{\partial \Delta\hat{z}_i / \Delta y}{\partial t}\right)^2\right) \quad \textbf{(15)}$$

Conform solving $\hat{s}_z$ in Eq.5, $\hat{s}_{zt}$, the contribution of changes of gradients in $\hat{z}_i$ is determined with spatial-averages from neighbouring domains. Solving migration rate c with Eq.15 is based on comparing two soundings at different dates. The sign of c can be obtained by minimizing the difference between a mathematical kinematic wave model and observed bed levels. To reduce discretization errors, the period between soundings should be smaller than $0{,}15L/c$.

3. Application to the river Waal

To evaluate the procedure as described above and to illustrate the resulting morphological parameters, a case study of the river Waal is added. The bed levels of the river Waal are observed with multi-beam echo-soundings, and projected on a 5 m x 5 m grid that is orientated in the direction of flow. Note that with depths of 5 m at average flow, these observations do not include ripples properly. As stated above, the observed bed levels are averaged and processed per domain, which should be long enough to include sufficient fluctuations by bed forms, and short enough to discretize the variations in bed-form averaged levels of crossings and bends. For the river Waal, the appropriate domains were defined (Fig.4) with a length of L_x= 500 m (about ten times the bed-form length) in the direction of flow, and an width of L_y=50 m (0,2 times the bankfull width).

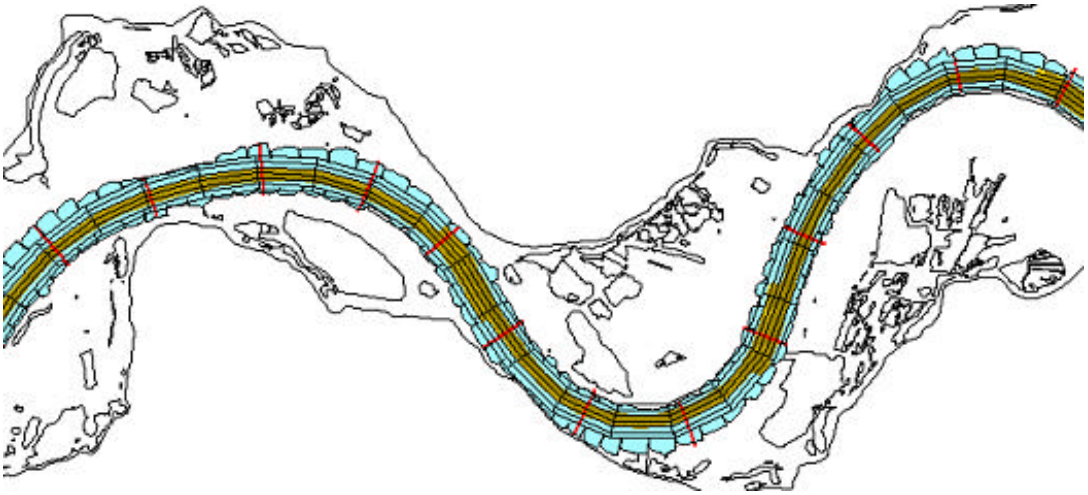

Figure 4 Example of grid with averaging-domains for the river Waal.

Now, for every domain sufficiently filled with data, two types of variables were generated; the *slowly varying* spatial average $\hat{z}_i$ and standard deviation $\hat{s}_z$, and the *rapid* bed level changes that are associated with the bed-form parameters amplitude H, wave length L, orientation $\langle$ and migration rate c. The category of slower morphodynamics can be used to calibry and verify operational models for two-dimensional river morphology. When available, $\hat{z}_i$ (and $\hat{s}_z$) enable a wide range of one-dimensional and two-dimensional morphological analyses on seasonal or decadal developments in bed level.

An example of local, seasonal developments is given in Fig.3 (Taal, 1998), where bed-form averaged levels $\hat{z}_i$ are shown before and after dredging in an inner bend and deposition in the downstream outer bend. The disturbances caused by dredging and deposition propagate downstream as a trench and hump respectively. As a result, the inner bend recovers within a period of ten months. In the outer bend however, two processes can be recognized; an initial recovery of the local deposition followed by a temporal lowering due to passage of the trench that originates from the upstream dredging.

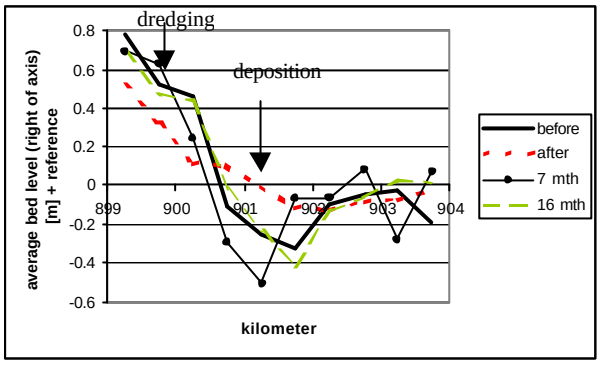

Figure 3-a Bed-form averaged profile before and after dredging and deposition.

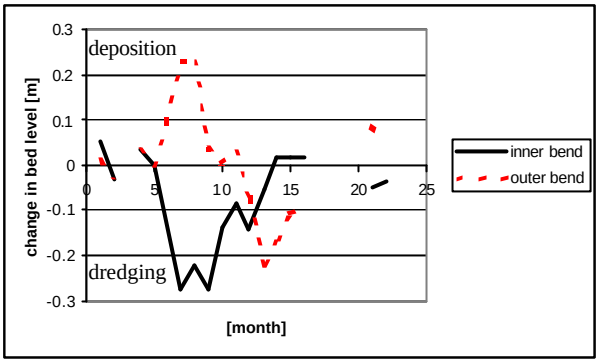

Figure 3-b Bed-form averaged changes in the inner and outer bend.

In Fig.4, representative, time-averaged cross-sections for low flow and high flow seasons are shown. This suggests that during floods, sedimentation in inner bends and erosion of crossings develops, probably due to a redistribution of flow and sediment transport. Additionally to this redistribution, local exchanges between flood plain and main channel can contribute to bed level changes. For optimal river management, operational models are required that simulate and predict these processes. Data analyses with the approach described in the previous section enables developing such models.

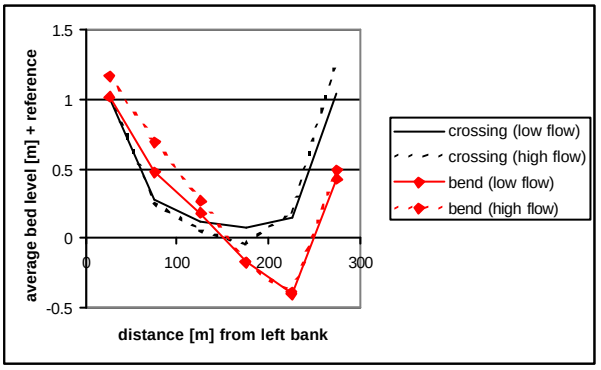

Figure 4 Cross-sections averaged over low flow or high flow season.

An application on a larger scale concerns time-averaged values of level $\hat{z}_i$ and standard deviation $\hat{s}_z$ along a significant part of the river Waal (Fig.5) during a period of low flow. For an automated processing of this relatively large data volume, an *Arcview* application was developed based on the approach of the previous section. In Fig.5, quasi-equilibrium values of bed levels $\hat{z}_i$ in the navigable profile are determined. These quasi-equilibrium values of level $\hat{z}_i$ can change due to long term developments on a decadal time-scale. The trend in spatial deviation $\hat{s}_z$ indicates the contribution of river bends in the upper part of the river Waal.

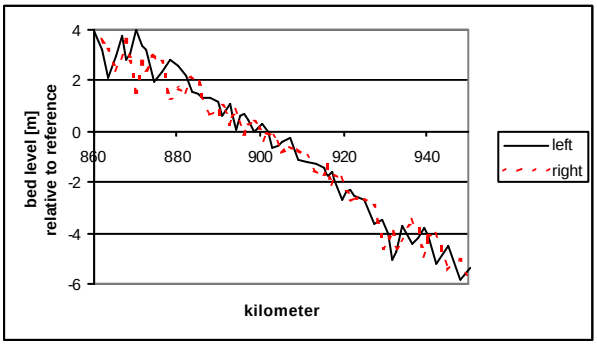

Figure 5-a Time-averaged, bed-form averaged longitudinal profile of $\hat{z}_i$ in the river Waal.

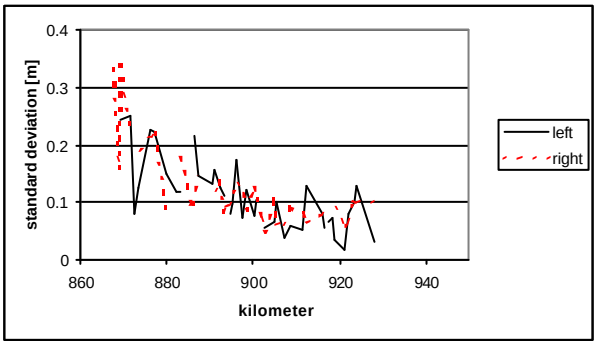

Figure 5-b Standard deviation $\hat{s}_z$ of time-averaged profile in the river Waal.

Apart from relatively slow changing bed-form averaged levels, the bed form parameters H, L, $\langle$ and c are determined that represent small-scale morphodynamics. An example of bed form parameters during a flood wave is shown in Fig.6, which is based on daily observations of bed levels over a length of 1 km (left is outer bend, right is inner bend). The discharge through the main channel is represented with a black line. The bed form parameters respond rather quickly to the varying conditions of flow.

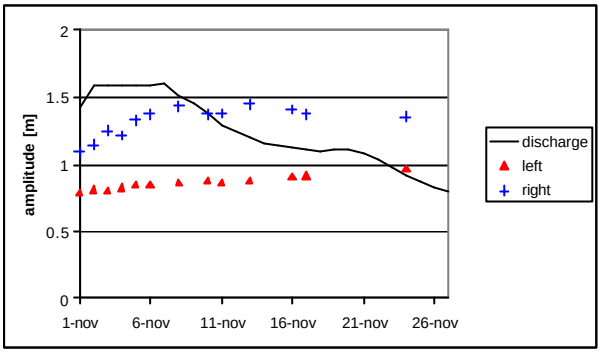

Figure 6-a Variation in amplitude.

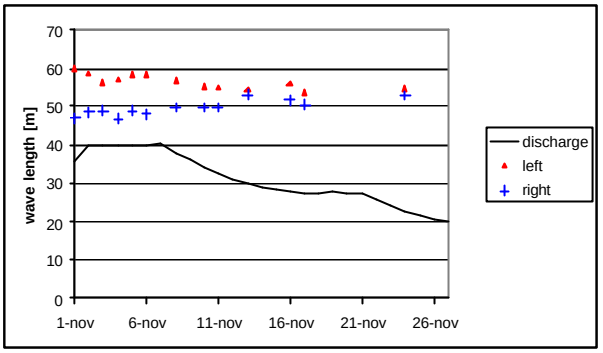

Figure 6-b Variation in wave length.

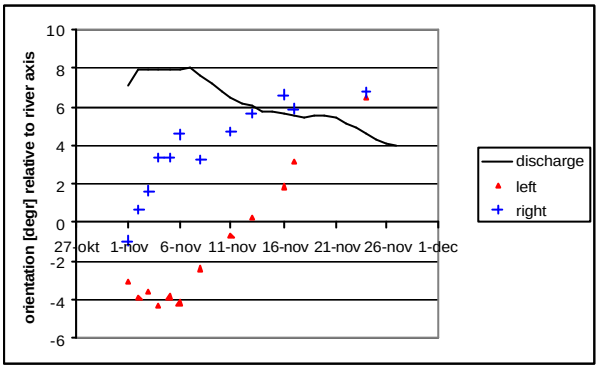

Figure 6-c Variation in orientation (positive is towards the inner bend).

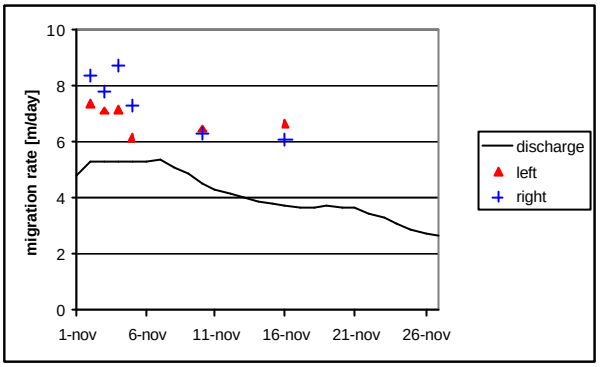

Figure 6-d Variation in migration rate.

These bed form parameters can be interpretated as follows. The wave length L and migration rate c can be combined in a time scale $T=L/c$ to represent with the amplitude H the rapid and local changes in bed level. The information on amplitude H and wave length L (Figs 6-a and 6-b) could be combined in a bed-form steepness for bed roughness predictors (e.g. Sieben, 2003). At this stage, however, it should be verified whether combining statistically equivalent parameters yield a physically realistic result. Although the trend in orientation (Fig.6-c) indicates a growing bed-load transport towards the inner bend, again it should be verified whether a statistically equivalent parameter represents such a physical process.

4. Distinction of migrating bed forms

As described above, a single set of representative bed-form parameters is determined for every domain in the river bed. However, the observed bed levels often consist of different type of bed deformations. Since ripples are excluded in the coarse grid used, the relevant types of deformation are *migrating* dunes and *steady* scouring holes induced at groyne heads. These contributions are illustrated in Fig.7.

Figure 7-a Observed level with migrating and steady bed forms

Figure 7-b Steady bed forms only (time-averaged bed level).

Figure 7-c Migrating bed forms only (Fig.7-a relative to Fig.7-b)

Hence, in a spatially non-uniform mode, steady bed deformations contribute to observed bed levels. In contrast with bed-form identifications of Wilbers and Ten Brinke (1999) no expert-driven filtering is applied. Therefore, to separate these contributions of migrating dunes and steady scouring holes explicitly, the following procedure was developed. Conform Fig.7, after time-averaging of a sufficient number of observations, the contribution of migrating dunes can be suppressed. Then, with the formulae as described above, the bed-form parameters H_s, L_s and $\langle_s$ can be obtained (with index *s* for steady) from the time-averaged bed level. Secondly, observed bed levels, including both type of bed deformations, are processed yielding bed-form parameters H_{tot}, L_{tot}, $\langle_{tot}$ and c_{tot} (with index *tot* for total). Now, with the theorem of *Parseval*, the bed-form parameters H_m, L_m, $\langle_m$ and c_m (with index *m* for migrating)can be found with

$$H_m = H_{tot}\sqrt{1-\left(\frac{H_s}{H_{tot}}\right)^2}\ ;\ L_m = L_{tot}\sqrt{\frac{1-\left(\frac{H_s}{H_{tot}}\right)^2}{1-\left(\frac{L_{tot}}{L_s}\right)^2\left(\frac{H_s}{H_{tot}}\right)^2}}\ ;\quad c_m = \frac{c_{tot}}{1-\frac{H_s}{L_s}\frac{L_{tot}}{H_{tot}}}\ ;$$

$$\text{and}\ \sin(2q_m) = \left(1-\left(\frac{H_s}{H_{tot}}\right)^2\left(\frac{L_{tot}}{L_s}\right)^2\right)^{-1}\left(\sin(2q_{tot})-\left(\frac{H_s}{H_{tot}}\right)^2\left(\frac{L_{tot}}{L_s}\right)^2\sin(2q_s)\right) \qquad \textbf{(16)}$$

To illustrate the correction according to Eq.16, this procedure is applied to six bed levels in the river Waal, that were observed during an eight-month period of low flow in 2003. In this example, with unfortunately a poor averaging of six series, the corrected amplitude of migrating deformations decreased from 10 to 20 % and the correction in wave length ranged from –10 to + 10 %. Some results are presented in Fig.8 for the river Waal, with *m* for migrating and *s* for steady bed forms. Probably due to the preference of upstream-moving, loaded vessels for the left-hand side, amplitudes in this part of the cross-section tend to be smaller and migration rates tend to be higher (Fig.8-a). During floods, this a-symmetric interaction between navigation and bed levels is not significant.

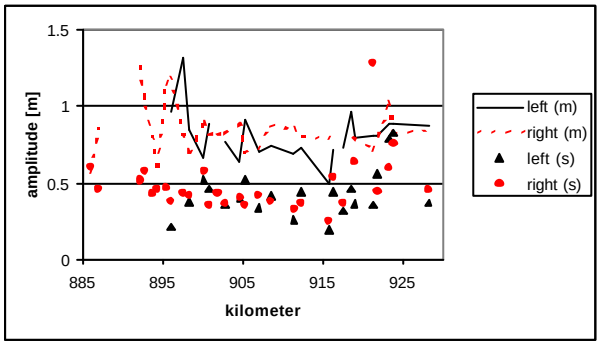

Figure 8-a Longitudinal profile of amplitude in migrating bed forms.

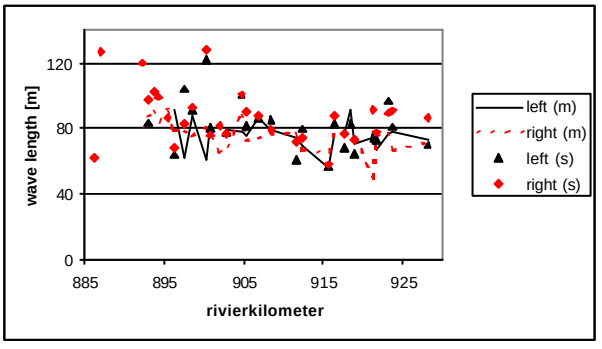

Figure 8-b Longitudinal profile of wave length in migrating bed forms.

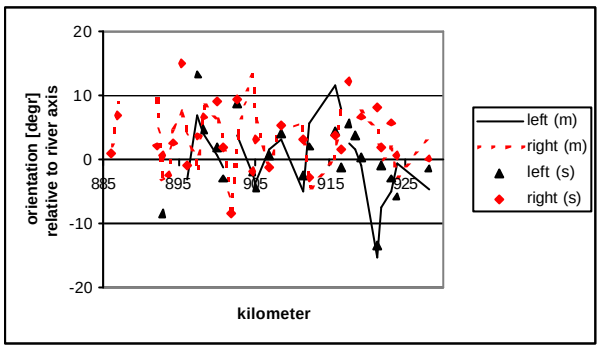

Figure 8-c Longitudinal profile in orientation of migrating bed forms (positive to right bank).

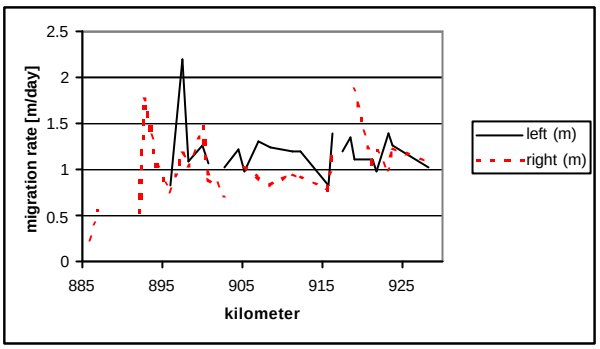

Figure 8-d Longitudinal profile of migration rate.

5. Conclusions

Using a concept of statistical equivalency, a procedure was developed and tested to characterize the relatively slow dynamics of bed-form averaged levels, and the relatively rapid changes in bed forms. This concept can be an efficient tool to construct a database that enables analyses of temporal and spatial variations in bed levels. The resulting parameters correspond with theoretical concepts of operational hydraulic and morphological models and hence enable a proper calibration and verification. Furthermore, prototype knowledge can be expanded by exploring the information obtained, for example to

i) predict the recovery of bed forms and bed-form averaged levels after local dredging and deposition using time-scales and equilibrium values
ii) analyse groyne-related scouring holes
iii) predict unsteady and/or non-uniform values of bed roughness
iv) describe lateral sediment transport using the orientation of bed forms

Acknowledgments

This study was carried out by commission of Mr Smedes from Rijkswaterstaat Directie Oost-Nederland mainly, for the improvement of morphological predictions in the decision support system for dredging. Messrs Van Essen, Schutte en Streekstra from RIZA are acknowledged for laborious *Arcview* analyses, keen Fortran programming and adequate *Arcview* automation respectively.

References

Cramér, H. en M.R. Leadbetter (1967); *Stationary and related stochastic processes, sample function properties and their applications*, Wiley Series in Probability and mathematical statistics, John Wiley and Sons, Inc.

Nordin, C.F. (1971); Statistical properties of dune profiles, Sediment transport in alluvial channels, Geological Survey Professional Paper 562-F.

Rijn, L.C. van (1984); Sediment transport, part III: Bed forms and alluvial roughness, Journal of Hydraulic Engineering, ASCE, Vol.110, No.12, pp.1733-1754.

Sieben, J. (2003); Estimation of effective hydraulic roughness in non-uniform flow, XXX IAHR Congress Inland waters: research, engineering and management, Theme C, Vol.II, pp.17-24.

Sloff, C.J.; M. Ververs; J. Boelens; D.Waardenburg and J. Sieben (2002); Morfologische module voor BOS Baggeren fase 2 (in Dutch), Q3261, WL Delft Hydraulics, Resource Analysis, RIZA.

Sloff, C.J.; M. Bernabè and T. Bauer (2003); On the stability of the Pannerdensche Kop river bifurcation, 3rd IAHR Sympos. on River, Coastal and Estuarine Morphodynamics, pp.1001-1011.

Taal, M.C. (1999); Metingen Proef Morfologie, RWS Directie Oost-Nederland,W-BG-99110.

Vries, M. de G.J. Klaassen en N. Struiksma (1990); On the use of movable-bed models for river problems: a state-of-the-art", door, in International Journal of Sediment Research, Vol.5 No 1

Wilbers, A.W.E. and W.T.M. ten Brinke (1999); Development of subaqueous dunes in the Rhine and Waal, the Netherlands, a preliminary note, IAHR Symposium on River, Coastal and Estuarine Morphodynamics, pp.303-312, Italy.